

PACS numbers: 42.55.Lt; 52.50.Jm
DOI: 10.1070/QE2015v045n10ABEH015842

Study of spectral characteristics of radiation from a thermal wake of a pulsating optical discharge in a supersonic air flow

A.N. Malov, A.M. Orishich, Ya.S. Terent'eva

Abstract. **The spectral characteristics of the thermal wake of a pulsating optical discharge (POD) in a supersonic air flow are studied. The POD is stimulated by radiation of a mechanically *Q*-switched, repetitively pulsed CO_2 laser with a pulse repetition rate of 7–150 kHz and a power up to 4.5 kW. The flow is produced by means of the supersonic aerodynamic MAU-M setup having a conic nozzle with a critical cross-section size of 50 mm, the Mach number being 1.3–1.6. We describe in detail the system of optical diagnostics that allows the detection of the spectrum of the weak thermal wake glow against the background of high-power POD radiation. The glow of the thermal wake is due to the emission of light by atoms and ions of nitrogen and oxygen, carried by the flow in the form of hot low-density gas clouds (caverns). The wavelengths of the thermal wake emission and the data on the transitions, corresponding to the spectral lines are presented.**

Keywords: *pulsating optical discharge, thermal wake, cavern, supersonic air flow.*

1. Introduction

One of the promising lines of laser radiation applications is the study of the physical processes that determine the properties of the pulsating optical discharge (POD) in a supersonic air flow. These studies are important for the solution of the problems, arising in the control of aerodynamic parameters of aircrafts, plasma chemistry, etc. [1–3]. The dynamics of laser spark formation in still air and the hydrodynamic relaxation of a hot gas cloud are studied well enough [4, 5]. The effects observed were the formation of a virtually spherical shock wave and the relatively slow radial expansion of the glowing region of the heated ionised gas or plasma. In Refs [6–10] the POD was ignited in the focus of a beam from a repetitively pulsed CO_2 laser in a supersonic argon jet and affected the flow in a similar way as a cw optical discharge. Grachev et al. [11] present the typical radiation spectrum with high resolution (0.01–0.005 nm) for the POD ignited by irradiating steel placed in an air flow.

The creation of a high-power, repetitively pulsed CO_2 laser [12] opened the possibility of igniting the POD in a supersonic air flow from real aerodynamic setups and of studying the characteristics of the produced thermal wake. At a laser power up to 4 kW and a pulse repetition rate up to 120 kHz the authors of Ref. [13] obtained the values of the mean mass temperature inside the wake ~120 °C–150 °C in the immediate vicinity of the plasmoid (at a distance of ~5 mm). In these experiments, the glow of the thermal wake (having the size of nearly 50 mm) was also observed that could not be determined by the abovementioned temperature of the gas in the jet. However, this glow could be related to the emission from caverns that arise in the gas flow in the process of pulse-periodic gas breakdown by laser radiation and survive during ~100 μs. In subsequent papers [14–16] the structure of the thermal wake was studied. Using the shadow method with the exposure time 0.15 μs, the shape, size and velocity of caverns were determined, and the glow of such formations in the thermal wake was recorded integrally over the spectrum.

Despite a large number of papers devoted to the optical breakdown in air, there is still no clear understanding of the elementary physical processes that determine the lifetime and the energy relaxation of plasma. For example, the experimental studies of the plasma emission spectra were carried out integrally over the time [17–19], or by measuring the glow in individual regions of a continuous spectrum [20], which did not allow the investigation of the process that determine the properties of the late stage of cloud evolution when the adiabatic expansion turns into the isobaric one.

The aim of the present work was to obtain the data on the spatio-temporal spectral characteristics of the optical radiation emitted by the supersonic air jet after the effect of the POD with high spectral resolution.

2. Experimental setup and measurement techniques

We used a mechanically *Q*-switched, repetitively pulsed CO_2 laser with a pulse repetition rate up to 150 kHz and a power up to 4.5 kW [12]. The pulse power of the laser was 60–200 kW depending on the modulation conditions. The schematic of the experiment is presented in Fig. 1. The experimental studies were carried out with a supersonic aerodynamic MAU-M setup having a conical nozzle (*1*) with the critical size of the flow cross section 50 mm (*2*), the Mach number being 1.3–1.6. Through the ZnSe lens (*5*) with a focal length 63 mm, laser radiation was directed to the axis line of the supersonic jet perpendicularly to the gas flow. The spot diameter in the focus of the lens amounted to 100–150 μm, which provided a peak intensity $(7–15)\times10^8$ W cm^{-2} in the optimal mode of laser operation and produced an optical breakdown of air [region (*3*)] in the supersonic jet. The laser

A.N. Malov, A.M. Orishich, Ya.S. Terent'eva S.A. Khristianovich Institute of Theoretical and Applied Mechanics, Siberian Branch, Russian Academy of Sciences, ul. Institutskaya 4/1, 630090 Novosibirsk, Russia; e-mail: laser@itam.nsc.ru

Received 20 April 2015; revision received 10 August 2015
Kvantovaya Elektronika **45** (10) 973–978 (2015)
Translated by V.L. Derbov

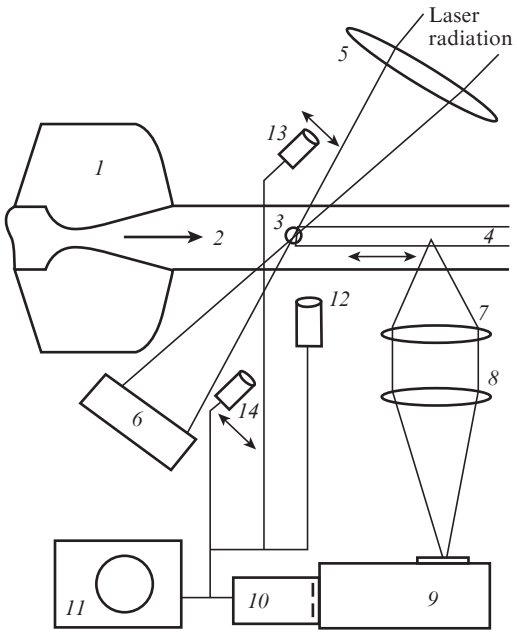

Figure 1. Schematic of the experiment:
(*1*) conical nozzle; (*2*) supersonic flow; (*3*) region of optical breakdown in air; (*4*) thermal wake; (*5*) ZnSe lens; (*6*) calorimetric power meter; (*7*, *8*) lenses of the optical tract; (*9*) CCS-200 spectrometer; (*10*) CCD camera; (*11*) digital oscilloscope; (*12*) coaxial photodetector; (*13*, *14*) FD-24K photodiodes.

radiation outgoing from the jet and the plasma formation zone was absorbed by a calorimetric NOVA 2 power meter (*6*) with the limit of measured power up to 5 kW. Figure 2 presents a photograph of the working zone of the setup with the optical discharge in the supersonic air flow. One can see the nozzle exit section, a bright spherical plasmoid and a thermal wake with a weaker glow, which becomes somewhat brighter towards the end of the wake.

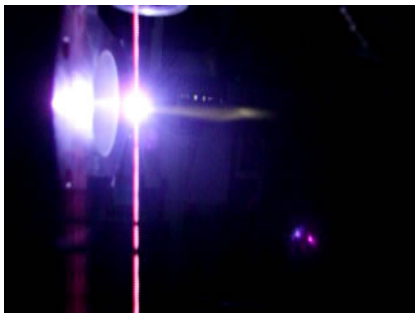

Figure 2. Photograph of the working section of the setup with the POD switched on.

To perform the visual observation of the plasma formation process in the supersonic jet and the thermal wake created by it, the setup was equipped with an optical diagnostic system. The optical scheme used to measure the weak signal of the thermal wake against the background of a high-power glow of the plasmoid included the optical tract (*7*, *8*), transmitting the image of a space point in the thermal wake (*4*) onto the entrance slit (*9*) of the recorder. The emission spectrum of the thermal wake was measured using a CCS-200 spectrometer with the spectral resolution not exceeding 2 nm, limited by the necessity to use the high-speed mode of the camera operation with the minimal time of its gate being open up to 10 μs and the maximal frame rate, each frame recording a wide interval of wavelengths (245–1050 nm). The optical system provided the spatial resolution ~100 μm in the volume of the thermal wake. To measure the dynamics of the energy absorption in the zone of the optical discharge we used FD-24K photodiodes (*13*, *14*), detecting the incident and transmitted radiation, respectively, and a coaxial FK-22 photo detector (*12*), detecting the light from the plasmoid. An oscilloscope (*11*) displayed the electric signals from the photodetectors.

To measure the glow spectrum of the caverns in the thermal wake we developed a special electronic circuit allowing the selection of the weak radiation from the wake against the background of the high-power glow of the plasmoid itself. This circuit produced the control pulse to switch on the spectrometer only at the moment when the cavern passes the measuring volume, determined by the lenses (*7*) and (*8*) (Fig. 1). The radiation in the spectrometer was integrated over this time and the light produced by a large (50–100) number of caverns, passed through the registration region, was accumulated. The spectrometer operation time for each switching on was 10–15 μs. This increased the sensitivity of the spectrometer to the required level and provided its isolation from the high-power light of the plasmoid. The interpretation of the spectra was performed using the data of Refs [17, 19, 21].

3. Experimental results and discussion

Figure 3 shows typical oscillograms of the incident and transmitted laser radiation, as well as the plasma glowing in the supersonic air flow. One can see that the bright glow lasts less than 1 μs and its intensity essentially (by a few orders of magnitude) exceeds the intensity of the thermal wake glow. During the next 100 μs a hot strongly rarefied cloud (a cavern) moves in the flow by the distance ~50 mm. Figure 4 presents a typical structure of shock waves and caverns of the thermal wake, formed in the supersonic air flow with a POD switched on (the frequency 60 kHz, the recording duration 150 ns). One can see that the thermal wake is a sequence of caverns, their boundaries changing their shape in the process of motion, due to which their cooling is not only diffusive, but also convective. For the flow velocity 500 m s^{-1} the separation between the caverns amounted to ~8.5 mm and their diameter was equal to 3–4 mm. Thus, a cavern passes the site of measurement during ~6 μs. For the time of the spectrum

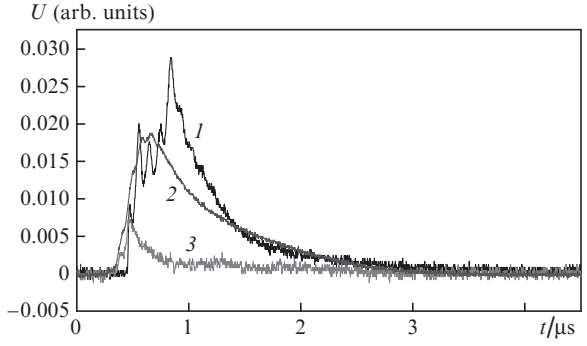

Figure 3. Oscillograms of (*1*) a plasmoid integral glow and laser radiation pulses (*2*) incident and (*3*) transmitted through the plasmoid.

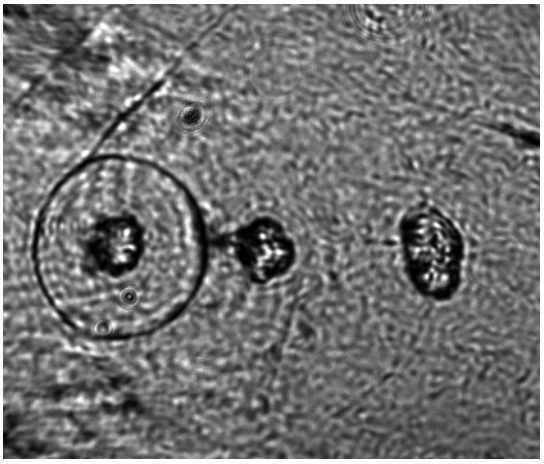

Figure 4. Shadow photograph of the structure of caverns and shock waves during the POD formation in a supersonic air flow. The registration time is 0.15 μs, the flow velocity is 500 m s^{-1} and the frequency is 60 kHz.

recording 10–15 μs the spectrum was measured with the appropriate choice of the distance and the switch-on time of the CCS-200 spectrometer. Under these conditions, in order to eliminate the influence of the plasma glow on the measurement of the cavern emission spectrum, the time interval between two plasma shots was chosen to be longer than 50 μs (the corresponding pulse repetition rate being less than 10 kHz). The spectrum was measured in a few points, both in the region of the plasmoid formation and along the thermal wake (at the distances 12, 25 and 50 mm from the plasmoid centre).

Figure 5 presents the spectrum of the plasmoid emission. Note that during the recording of this spectrum, i.e., during the camera operation time (~10 μs) the glow is averaged over all initial stages of the plasmoid development. Thus, the formation of the spectrum is due to different processes that lead to the appearance of strong spectral lines of molecules, atoms and ions of nitrogen and oxygen that emit radiation in the UV, visible, red and near-IR regions.

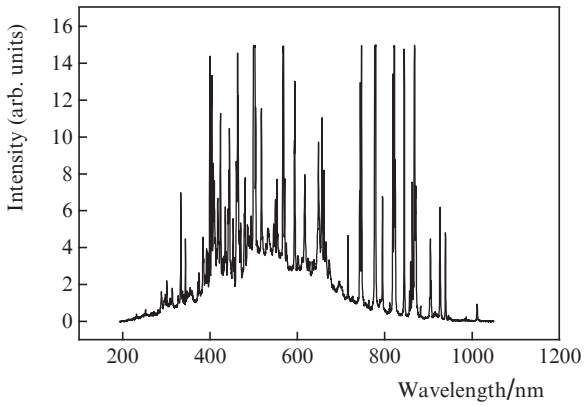

Figure 5. Characteristic spectrum of plasmoid emission.

Thus, according to the data [6], under the conditions of our experiment, i.e., the pulse energy 0.25 J, the transition of fast adiabatic spreading and cooling of the hot plasma after the breakdown to the slow isobaric spreading and cooling occurs in 1–2 μs. During this time, the intense glow is observed (see Fig. 3), making the main contribution into the formation of the plasmoid spectrum.

At the impact moment, corresponding to a laser pulse maximum (~200 ns), the prevailing processes in the presence of hot electrons are ionisation, dissociation and excitation of molecules, atoms and ions. At the stage of adiabatic expansion of the cloud, since the temperature of electrons is still high enough, the ionisation and dissociation of molecules continue. The growth of the electron concentration enhances the processes of electron quenching and excitation exchange between different multiplets. As a result, a variety of vibrational transitions are present in the spectrum of molecular emission, and the spectrum of N II nitrogen ions ehibits different electronic states and multiplets with the spin values 2, 1, and 0.

For more detailed analysis of elementary physical processes in the plasmoid and caverns Tables 1–3 present the characteristics of the electronic states of molecules, atoms and ions, corresponding to the observed line spectrum.

Note that practically each multiplet consists of several lines with the wavelengths differing by less than 1 nm. The spectrometer does not resolve these lines, so Tables 1–3 present the wavelength of the transition, closest (within the accuracy of 0.5 nm) to the spectral position of the intensity maximum of the band, corresponding to the glow of this multiplet. Moreover, within the resolution of the instrument, the overlap of possible different multiplets and even of different

Table 1. Electronic transitions of atoms for the emission spectrum presented in Fig. 5.

Emitter	Wavelength/ nm	Transition	Multiplicity	Intensity
N II	404.9	2p3d–2p4f	$^3F^0-{}^3G$	Very strong
	423.9		$^3D^0-{}^3F$	Strong
	654.4	2p3d–2p4p	$^3D^0-{}^3D$	Weak
	332.8 (2)	2p3p–2p4s	$^3D-{}^3P^0$	Strong
	384.2 (3)		$^3P-{}^3P^0$	Strong
	391.9 (4)	2p3p–2p3d	$^1P-{}^1P^0$	Weak
	444.7		$^1P-{}^1D^0$	Strong
	593.8		$^3P-{}^3D^0$	Very strong
	343.7	2p3s–2p3p	$^1P^0-{}^1S$	Strong
	399.5		$^1P-{}^1D$	Very strong
	463.0		$^3P-{}^3S$	Very strong
	567.6		$^3P^0-{}^3D$	Very strong
		2p3p–2p3d	$^3D-{}^3F$	
			$^3P-{}^3P^0$	
	499–502	2p3s–2p3p	$^5P-{}^5P^0$	Very strong
			$^3P^0-{}^3S$	
		$2s2p^23s-2s2p^23p$	$^5P-{}^5P^0$	
		$2s^22p3p-2s^22p3d$	$^3S-{}^3P^0$	
	517.3 (5)	$2s2p^23p-2s2p^23p$	$^5D^0-{}^5F$	Strong
N I	517.6 (5)	$2s2p^4-2s^22p^24p$	$^4P-{}^4S^0$	Strong
	744.2	$2p^23s-2p^23p$	$^4P-{}^4S^0$	Very strong
	821.1		$^4P-{}^4P^0$	Weak
	862.9		$^2P-{}^2P^0$	Weak
	868.0		$^4P-{}^4D^0$	Strong
	904		$^2D-{}^2F$	Weak
	938.6		$^2P-{}^2D$	Weak
O II	517.6 (5)	$2p^23p-2p^23d$	$^2P^0-{}^2P$	Strong
O I	715.6	$2p^33s-2p^33p$	$^1D^0-{}^1D$	Weak
	777.3		$^5S-{}^5P$	Very strong
	794		$^3D^0-{}^3F$	Weak
	844.6		$^3S-{}^3D$	Weak
	926.3	$2p^33p-2p^33d$	$^5P-{}^5D^0$	Weak

Table 2. Electronic transition of atoms for the emission spectrum presented in Fig. 6b.

Emitter	Wavelength/ nm	Transition	Multi-plicity	Intensity
N I	664.4	$2p^23p-2p5s$	$^4D^0-^4P$	Weak
	742.3–746		$^4P-^4S^0$	Very strong
	821.1	$2p^23s-2p^23p$	$^4P-^4P^0$	Very strong
	869.1		$^4P-^4D^0$	Very strong
O I	615.5	$2p^33p-2p^34d$	$^5P-^5D^0$	Weak
	715.5		$^1D^0-^1D$	Weak
	777.3	$2p^33s-2p^33p$	$^5S-^5P$	Very strong
	844.6		$^3S-^3D$	Strong
N II	499.4	$2s2p^23s-2s2p^23p$	$^5P-^5P^0$	Weak
		$2s^22p3p-2s^22p3d$	$^3S-^3P^0$	Weak
	567.3	2p3s-2p3p	$^3P^0-^3D$	Weak
	615.5	2p3d – 2p4p	$^3F^3-D^0$	Weak
	648.2	2p3s – 2p3p	$^1P^0-^1P$	Weak

Table 3. Electronic transition of molecules for the emission spectrum presented in Fig. 5.

Emitter	Wavelength/ nm	Transition	Vibrational state	Intensity
N_2^+ (Janin–d'Incan)	245.5	$D^2\Pi_g-A^2\Pi_u$	(2.2)	Very weak
	251.6		(3.3)	Very weak
	344.7		(23.16)	Weak
N_2^+ (first negative system)	383.5 (3)	$B^2B_2\Sigma_u^+-X^2\Sigma_g^+$	(3.3)	Strong
	385.7 (1)		(2.2)	Strong
	391.4 (4)		(0.0)	Weak
N_2 (second positive system)	297.6	$C^3\Pi_u-B^3\Pi_g$	(2.0)	Very weak
	313.6		(2.1)	Very weak
	326.8		(4.4)	Weak
	333.8 (2)		(1.1)	Strong
	385.7 (1)		(4.7)	Strong
	394.3		(2.5)	Weak
	399.8		(1.4)	Very strong
	409.4		(4.8)	Strong
N_2 (first positive system)	646.8	$B^3\Pi_g-A^3\Sigma_u^+$	(8.5)	Weak

electronic states was observed. A typical example of this situation is the strong emission of the N II ion with the wavelength ~500 nm and the bandwidth up to 3 nm (see Table 1). In Tables 1, 3 similar situations are labelled with similar figures from 1 to 5. In particular, the insufficient resolution does not permit an unambiguous conclusion about the presence of the N_2^+ ion emission (the first negative system), for which all lines to be observed overlap with the emission lines of the N II ion and the N_2 molecule (second positive system). One should take the above factors into account in the analysis of the spectra.

Note that the spectrum of the plasmoid appeared to be close to the emission spectrum of the high-current discharge, presented in Fig. 2 of Ref. [17]. In addition to discrete lines and bands, a continuous spectrum of emission is observed in the wavelength region near 500 nm. The position of the maximum of this band, evaluated within the frameworks of the blackbody radiation model with the spectral sensitivity of the instrument taken into account, corresponds to the radiation temperature ~5800 K, which is close to the results of Ref. [17].

In the analysis of the plasmoid spectrum, one can select the processes of cascade transition of electrons down from upper levels with the quantum number 4 (4s, 4p, 4f) with the emission of very strong lines, e.g.,4f → 3d ($^3F^0-^3G$), 3d → 3p ($^3P-^3D$, $^3D-^3F$, $^3P-^3P^0$), 3p → 3s ($^1P^0-^1S$, $^1P-^1D$, $^3P-^3S$, $^3P^0-^3D$). One can see that in this cascade the transitions conserving the spin $S = 1$ prevail. One can assume that the process of populating the levels of the atoms N I and O I involves both the excitation and dissociative recombination, the conditions for which can be implemented at the cavern boundary, where the plasmoid contacts with the cold surrounding air and cooled plasma.

Figures 6 and 7 present the emission spectra of caverns in the thermal wake at the distances 24 and 50 mm. For the flow velocity 500 m s^{-1} the time of cavern appearance at these distances amounted to 50 and 100 μs, respectively. Figure 6 shows the emission spectra at different values of the recording system sensitivity (differing by 50–100 times). From the spectra presented in Figs 5–7 one can see that the spectra of the cavern glow essentially change with time and considerably differ from the spectra of the plasmoid emission. At a low sensitivity (Fig. 6a) after 50 μs only five relatively strong lines are observed in the cavern glow in the IR region 700–900 nm. When the sensitivity is essentially increased, we could record the continuous spectrum in the region 400–600 nm and a few weak lines, but the strong lines were saturated. The low sensitivity is related to the fact that at the time of measure-

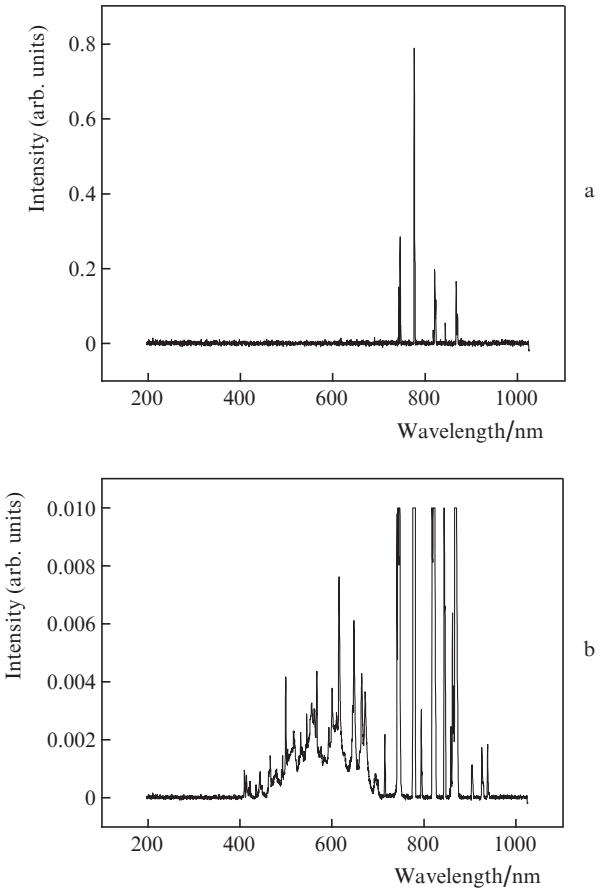

Figure 6. Spectra of the cavern emission in the thermal wake at a distance 24 mm from the centre of the plasmoid formation at (a) low and (b) high sensitivity of the measuring devices.

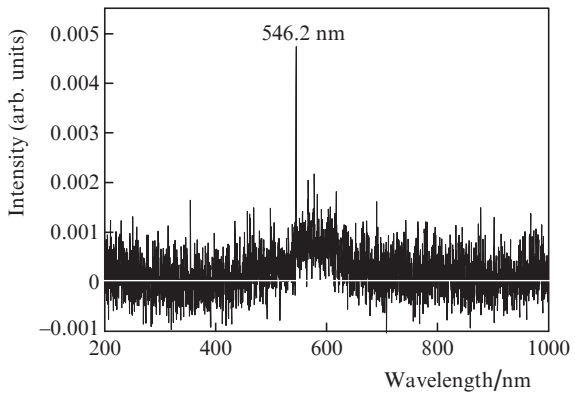

Figure 7. Spectrum of the cavern emission in the thermal wake at a distance 50 mm from the centre of the plasmoid formation.

ment the cavern flew over the measurement point at a certain distance, where the intensity of the recorded radiation was small. At the distance of 50 mm (in 100 μs from the moment of the cavern formation), with the sensitivity of the measuring system being maximal possible in our experiments, we managed to detect the cavern glow as a continuous spectrum and a single line (Fig. 7).

From the data of Table 3 it is seen that in the plasmoid the strong emission of the N_2 molecule (the second positive system, $C^3\Pi_u - B^3\Pi_g$) is present. In the cavern this emission is not detected. Of great interest is the glow of the N II ions, their emission being concentrated in the interval 322–567 nm. In the cavern at the distance 25 mm (in 50 μs) the emission of the N II ion is very weak and concentrated in the interval 500–648 nm (Table 2).

The specificity of the emission by the N I and O I atoms is of particular interest. In the plasmoid one can select only two very strong lines of N I and O I at wavelengths 744.2 and 777.3 nm, respectively. In the cavern after 50 μs (25 mm) strong emission of these lines remains and three more lines appear, i.e., the emission of five lines, relatively close in intensity, is observed (see Fig. 6a), namely, the lines of the N I atom (744.2, 821.1 and 869. 1 nm) for one electronic configuration $2p^23s - 2p^23p$ (multiplets $^4P - ^4S^0$, $^4P - ^4P^0$, $^4P - ^4D^0$) and the O I atom (777.3 and 844.6 nm) for the electronic configuration $2p^33s - 2p^33p$ (multiplets $^5S - ^5P$, $^3S - ^3D$). According to Ref. [17], the cold electrons can take part in the formation of the IR spectrum of the N I and O I atoms, providing the dissociative recombination of the plasma in the following basic processes:

$$N_2^+ + e \rightarrow N^* + N \rightarrow 2N + h\nu \text{ (746 nm, etc.)}, \quad (1)$$

$$O_2^+ + e \rightarrow O^* + O \rightarrow 2O + h\nu \text{ (777 nm, etc.)}. \quad (2)$$

In the cavern during the time up to 50 μs one can observe the weak emission of some lines of nitrogen ions, which is probably due to the recombination processes. The formation of the spectrum of the yellow-green band 450–750 nm (see Figs 6 and 7) can be determined [17] by the chemical reaction with the production of the nitrogen dioxide molecule in the decaying cavern at a late stage of its development, the distance being 25–50 mm (the times 50–100 μs) from the place of the plasmoid formation:

$$NO + O \rightarrow NO_2^* \rightarrow NO_2 + h\nu.$$

4. Conclusions

In the present paper we report the first experimental study of time variation (during up to 100 μs) of the POD emission spectrum in a supersonic air flow. In the analysis of the plasmoid spectrum, i.e., the initial stage of the POD, we recorded both the continuous emission spectrum in the region 200–290 nm and a variety of lines, belonging to neutral and ionised molecules and atoms of oxygen and nitrogen. We revealed the presence of the lines of the N II ion, caused by the cascade process of emission, mainly with spin conservation in the transitions from the upper shells, e.g., 4f → 3s.

An essential change in the spectrum under the transition from the adiabatic expansion, characterised by very intense glow, to the isobaric one is demonstrated. It is found that even in 50 μs after the cavern formation at the distance up to 25 mm downstream, its emission spectrum, alongside with the strong lines of the N I and O I atoms, probably caused by dissociative recombination of the ions N_2^+ and O_2^+, contains weak lines of the N II ion. It is found that at large distances the glow of the thermal wake is due to the glow of caverns in the region of the yellow-green band 450–750 nm at the isobaric stage of their evolution (up to 100 μs and the distance of 50 mm downstream), which can be determined by the chemiluminescence under the interaction of the NO molecules with the O atoms and the formation of the excited NO_2 molecules.

References

1. Ellinwood J.W., Mirels H. *Appl. Opt.*, **14** (9), 2238 (1975).
2. Tret'yakov P.K., Garanin A.F., Grachev G.N., Krainev V.L., Ponomarenko A.G., Tischenko V.N., Yakovlev V.I. *Dokl. Ross. Akad. Nauk*, **351** (3), 339 (1996) [*Doklady Physics*, **41** (11), 566 (1996)].
3. Akhmanov S.A., Rudenko O.V., Fedorchenko A.T. *Pis'ma Zh. Tekh. Fiz.*, **5**, 934 (1979) [*Sov. Tech. Phys. Lett.*, **5**, 387 (1979)].
4. Raizer Yu.P. *Lazernaya iskra i rasprostraneniye razryadov* (Laser Spark and Propagation of Discharges) (Moscow: Nauka, 1980).
5. Borzov Yu.V., Mikhailov V.M., Rybka I.V., Savishchenko N.P., Yur'ev A.S. *Inzh.-Fiz. Zh.*, **66**, 515 (1994) [*J. Eng. Phys. Thermophys.*, **66** (5), 449 (1994)].
6. Tret'yakov P.K., Grachev G.N., Ivanchenko A.I., Krainev V.L., Ponomarenko A.G., Tishchenko V.N. *Dokl. Ross. Akad. Nauk*, **336**, 466 (1994).
7. Bagayev S.N., Grachev G.N., Ponomarenko A.G., Smirnov A.L., Demin V.N., Okotrub A.V., Baklanov A.M., Onishchuk A.A. In: *Nauka i nanotekhnologii* (Science and Nanotechnologies) (Novosibirsk: Izd-vo SO RAN, 2007) p. 123.
8. Tishchenko V.N., Grachev G.N., Pavlov A.A., Smirnov A.L., Pavlov Al.A, Golubev M.P. *Kvantovaya Elektron.*, **38**, 82 (2008) [*Quantum Electron.*, **38**, 82 (2008)].
9. Sperber D., Schmid F., Eckel H.A., Fasoulas S. *Proc. 6th AIAA Flow Control Conf.* (New Orleans, Louisiana, USA, 2012).
10. Sperber D., Eckel H.-A., Steimer S., Fasoulas S. *Contrib. Plasma Phys.*, **52** (7), 636 (2012).
11. Grachev F.N., Medvedev A.E., Pinaev P.A., Tishchenko V.N. *Trudy V Vseros. Konf. 'Vzaimodeistvie vysokokonstentrirovannykh potokov energii s materialami v perspektivnykh tekhnologiyakh i meditsine'* (Proc. 5th All-Russia Conf. 'Interaction of Highly Concentrated Energy Flows with Materials in Perspective Technologies and Medicine' (Novosibirsk, 2013).
12. Malov A.N., Orishich A.M., Shulyan'ev V.B. *Kvantovaya Elektron.*, **41**, 1027 (2011) [*Quantum Electron.*, **41**, 1027 (2011)].
13. Malov A.N., Orishich A.M. *Pis'ma Zh. Tekh. Fiz.*, **38**, 32 (2012) [*Tech. Phys. Lett.*, **38** (1), 70 (2012)].
14. Malov A.N., Orishich A.M., Bobarykina T.F., Chirkashenko V.F. *Opt. Atmos. Okeana*, **25**, 244 (2012).
15. Malov A.N., Orishich A.M. *Kvantovaya Elektron.*, **44**, 83 (2014) [*Quantum Electron.*, **44**, 83 (2014)].

16. Bobarykina T.A., Malov A.N., Orishich A.M., Chirkashenko V.F., Yakovlev V.I. *Kvantovaya Elektron*., **44**, 836 (2014) [*Quantum Electron*., **44**, 836 (2014)].
17. Prokop'yev V.E., Ivanov N.G., Krivonosenko D.A., Losev V.F. *Izv. Vyssh. Uchebn. Zaved., Ser. Fiz.*, **56**, 60 (2013).
18. Bukin O.A., Il'yin A.A., Kul'chin Yu.N., Nagornyi I.G., Pavlov A.N., Bulanov A.V. *Kvantovaya Elektron*., **36**, 553 (2006) [*Quantum Electron*., **36**, 553 (2006)].
19. Camacho J.J., Poyato J.M.L., Díaz L., Santos M. *J. Phys. B: At. Mol. Opt. Phys*., **40**, 4573 (2007).
20. Kabanov S.N., Maslova L.I., Terekhova T.A., Trukhin V.A., Yurov V.T. *Zh. Tekh. Fiz*., **60**, 37 (1990) [*Sov. Phys. Tech. Phys*., **35**, 655 (1990)].
21. Wiese W.L., Smith M.W., Glennon B.M. *Atomic Transition Probabilites. Vol. 1. Hydrogen through Neon* (Washington, 1966) p. 153.